MICROSTRUCTURAL EXAMINATION OF V-4CR-4TI PRESSURIZED THERMAL CREEP TUBES - D. S. Gelles (Pacific Northwest National Laboratory)*

OBJECTIVE

The objective of this effort is to provide further understanding of processes controlling thermal creep in vanadium alloys.

SUMMARY

Two further failed thermal creep pressurized tubes of V-4Cr-4Ti tested at 700 and 800°C have been examined using optical microscopy and transmission electron microscopy in order to understand failure and creep mechanisms. These conditions represent lower stress states than were previously examined. Creep deformation at lower stress is shown to be controlled by sub-boundary formation and mis-orientation between sub-grains arising from climb of dislocations within the boundary.

PROGRESS AND STATUS

Introduction

Biaxial thermal creep microstructural response for V-4Cr-4Ti at 700 and 800°C was recently reported.[1] The present effort describes examination using optical microscopy (OM) and transmission electron microscopy (TEM) techniques of specimens at lower stress states that failed more recently. The OM examinations were intended to locate the failure sites and to begin evaluating the failure mechanism and the TEM microstructural examinations were intended to verify the controlling deformation mechanisms. The previous microstructural examinations had shown failure due to high local thinning with microstructures containing high densities of individual dislocations. Creep was therefore expected to be controlled by dislocation climb, in agreement with the high values for the stress dependence of secondary creep found.[2] Evidence for a well-defined dislocation cell structure was not found. The present results indicate a change in creep mechanism occurs for lower stress conditions.

Experimental Procedure

Details for the pressurized tubes examined in this and the previous study are provided in Table 1. Ring sections of specimens AR14 and AR16 were sectioned and punched to produce 3 mm curved disks in a manner similar to that done previously. Disks were thinned by grinding but evidence of the curvature was retained in order to be able to orient the microstructure relative to the stress state. Disks were then electropolished at low temperature using standard techniques to produce thin foils. Each disk was mounted in the microscope so that images could be related to the tube orientation and therefore the state of stress could be related to the microstructure. Dislocation imaging involved procedures that allowed identification of all $\frac{a}{2}$<111> Burgers vectors present.[3]

* Pacific Northwest National Laboratory (PNNL) is operated for the U.S. Department of Energy by Battelle Memorial Institute under contract DE-AC06-76RLO-1830.

Table 1. Test conditions for selected failed pressurized tube specimens of V-4Cr-4Ti (heat 832665).

Specimen ID	Temp. (°C)	Effective Stress (MPa)	Time to failure (hrs)	Effective mid-wall failure strain (%)
AR14	700	138.9	6667	14.8
AR15	700	158.8	2804	13.0
AR16	800	70.6	4029	51.9
AR17	800	92.6	864	13.6
AR18	800	117.7	578	24.1
AR19	800	136.8	242	14.7

Results

Macroscopic features

Photographs of tubes AR14 and AR16 using OM are shown in Figures 1a) and b), and c) and d), respectively. The tubes have been oriented to show the likely failure sites in the center of the tube. Tubes are 27.4 mm in length. In both cases failure appears to be due to formation of a longitudinal crack but the crack is shorter following testing at the higher temperature.

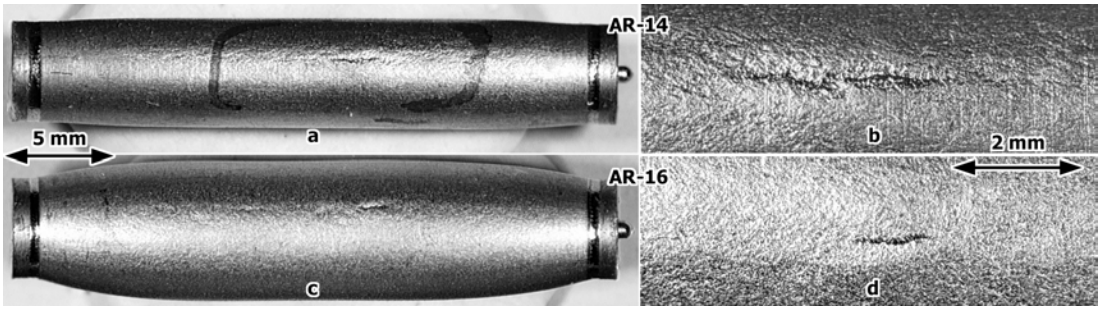

Figure 1. Failed pressurized tubes AR14 in a) and b) and AR16 in c) and d) shown with the likely failure sites face-on at low and intermediated magnifications.

The tubes were then sectioned in order to examine the failure sites from the inside of the tube. Failure features appeared similar to those in Figures 1b) and 1d).

Metallographic sections were then prepared in order to locate through-thickness cracks, Examples are provided in Figure 2 showing regions in specimens AR14 and AR16 that contain areas that have been reduced in wall thickness to the point of failure. From Figure 2, examples of grain elongation can be identified in each of the thinned sections, indicating that strain within grains reached high levels in comparison to grains in unthinned regions, where grains remained equiaxed, despite strains up to 50% as in specimen AR16. Therefore, local plasticity was very high prior to failure and failure was a result of that thinning.

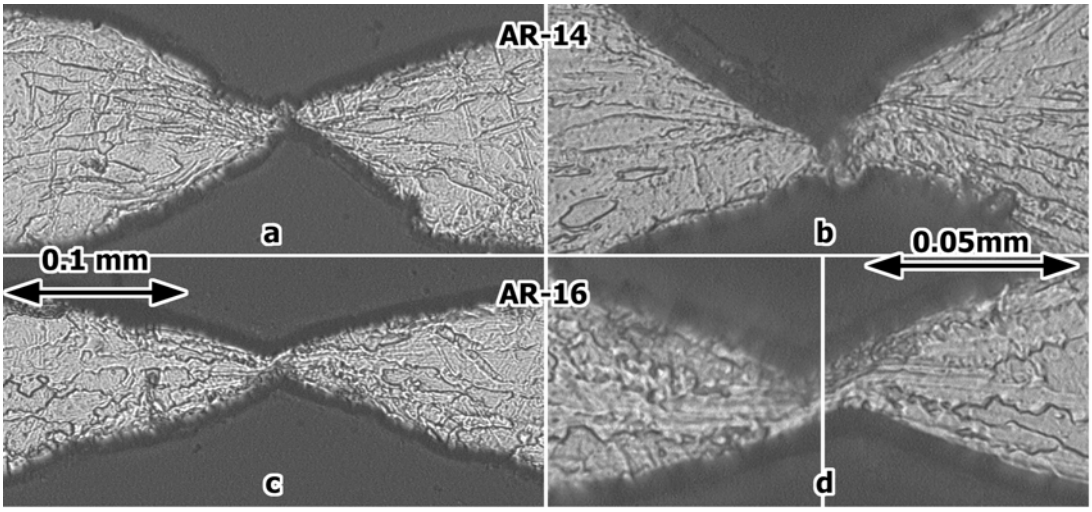

Figure 2. Optical metallography examples of thinned sections of specimens AR14 and AR16.

Microstructure

Specimens for TEM were successfully prepared from specimens AR14 and AR16 but thin area was limited. However, microstructures in these samples were quite different from those previously examined. Well defined sub-grain boundaries were found in each condition, with low dislocation densities between sub-grain boundary walls. Examples were found where the sub-grain boundary was connected to dislocations within sub-cells, perhaps indicating that these boundaries were beginning to break down. (Tests were continued for some time after failure, so the final stress state was reduced to zero before microstructural development was stopped.) However, the cells formed by these boundaries were often of very unusual shape. Examples at low magnification are provided in Figure 3 showing sub-grain boundary structures in AR-16 following creep at 800ºC. Although some sub-grains are equiaxed, many are unusually shaped such as one at the top of Figure 3a) and another on the upper left of Figure 3c. Initially the nature of the dislocations within sub-grains suggested that they were formed during preparation. Three vertical traces in Figure 3c) towards the upper left are indicative of dislocation migration within the foil. However, it is now understood that these dislocations were probably present following creep deformation.

Comparison of imaging conditions across a given sub-grain boundary demonstrated that the boundaries defined changes in tilt between adjacent sub-grains. Also, it was apparent that the dislocation structure within the sub-boundaries developed interesting patterns that clearly delineated the dislocations that made up the boundary. It appeared possible to analyze the dislocation arrays within a given sub-boundary in order to determine the character of the dislocations within the boundary, assuming that the Burgers vectors present were restricted to those that existed in the matrix. Therefore, several boundaries were imaged according to procedures previously described that allow determination of all Burgers vectors in a given area.[1,3]

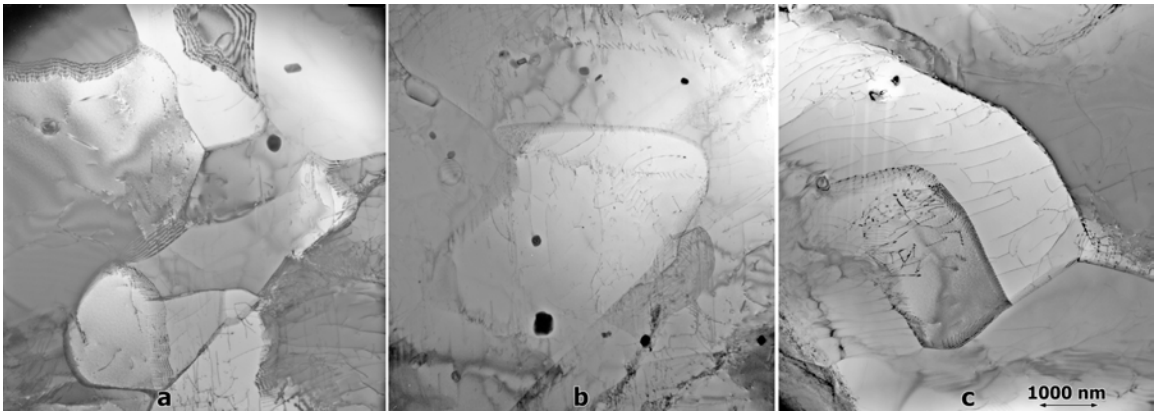

Figure 3. Examples of sub-grain boundaries in AR-16.

Examples of sub-grain microstructures are provided in Figures 4 to 7, 4 for condition AR-14 and 5 to 7 for AR-16. However, it should be noted that Figures 6 and 7 show the same sub-boundary but along two different sections. The figures have been prepared to allow identification of all $\frac{a}{2}$<111> Burgers vectors present, so three views of the same area are given, one in $01\bar{1}$ contrast and one in 200 contrast, both taken near a (011) orientation, and the third in either $\bar{1}10$ or $\bar{1}01$ contrast taken after a large tilt of the foil. Stronger contrast has been used in Figures 6c) and 7c) in order to emphasize that few dislocations appear in the boundary under this imaging condition. In each case, the foil orientation was determined at zero tilt and the microstructure could be related to the cylindrical axis of the pressurized tube, thereby allowing definition of the stress state. The mis-orientation across the sub-boundary is estimated for Figure 4 at 0.09° with the grain orientation near (001) for zero tilt. The mis-orientation across the sub-boundary for Figure 5 is 0.13° with the grain oriented near (133) for zero tilt and for Figures 6 and 7 the mis-orientation is estimated at 0.16° with the grain orientation near (001) for zero tilt. Note that rotational misorientation could not be determined to this degree of precision based on film records of the Kikuchi patterns. A stereographic triangle is inset for each figure sequence with a black dot to define zero tilt and an arrow to define the circumferential stress direction from that point. In all cases the tilt direction corresponded to the circumferential stress direction. In each of these figures, imaging with $\bar{g}$ = 200 as in b) should show all four of the possible $\frac{a}{2}$<111> Burgers vectors, whereas the other imaging conditions will only show two of the possibilities. With $\bar{g}$ = $01\bar{1}$ as in all a) figures, $\frac{a}{2}[1\bar{1}1]$ and $\frac{a}{2}[11\bar{1}]$ should be visible, whereas with $\bar{g}$ = $\bar{1}10$ as in the 4c), 6c) and 7c) figures, $\frac{a}{2}[\bar{1}11]$ and $\frac{a}{2}[1\bar{1}1]$ should be visible and with $\bar{g}$ = $\bar{1}01$ as in the 5c) figure, $\frac{a}{2}[\bar{1}11]$ and $\frac{a}{2}[11\bar{1}]$ should be visible. From these relationships, all Burgers vectors for dislocations present can be defined. However, it can be noted that fine dislocation arrays, such as in Figures 5, 6 and 7 have much weaker contrast using 200 contrast. See for example, Figures 5b), 6b) and 7b) where all dislocations should be equally visible.

Applying this Burgers vector analysis to Figure 4 through 7 provides several useful observations. In both the a) and b) figures for each of these micrograph series, a fine array of dislocations can be seen on each sub-boundary, having Burgers vector $\frac{a}{2}[\bar{1}11]$ in Figures 4, 6 and 7 and $\frac{a}{2}[1\bar{1}1]$ in Figure 5. But the closely spaced dislocations in Figure 4 (at the upper right) are oriented differently than those in Figures 6 and 7. A second array of more coarsely spaced dislocations appears in all images of Figures 6 and 7 indicating a Burgers vector of $\frac{a}{2}[1\bar{1}1]$. Some dislocations appear curved In Figure 7, showing that the screw verses edge component may be changing for a single dislocation in a sub-grain boundary. This change in character is probably associated

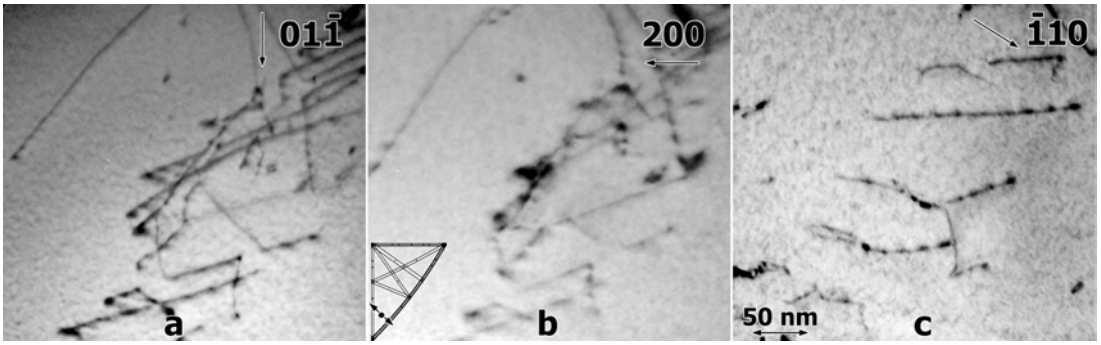

Figure 4. A sub-grain boundary in specimen AR-14 at 700ºC and 152 MPa.

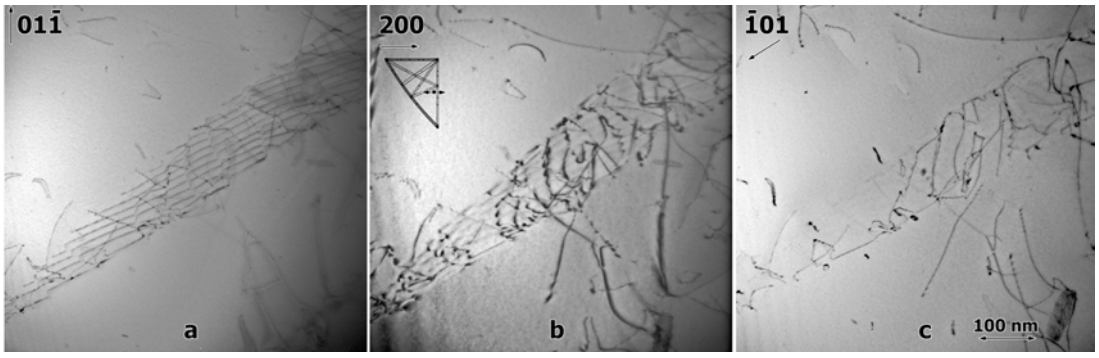

Figure 5. A sub-grain boundary region in specimen AR-16.

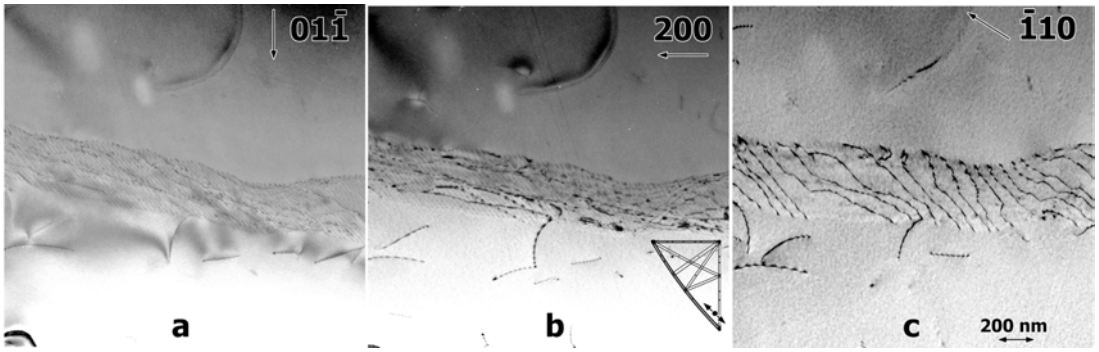

Figure 6. A sub-grain boundary in condition AR-16 at 800ºC and 77 MPa.

with the curvature of the boundary. Many coarsely spaced dislocations in subgrain boundaries exhibit zig-zag imaging. As these oscillations are not as apparent in matrix dislocation images, it is expected that the zig-zag behavior demonstrates network behavior with at least two different Burgers vectors represented, so that care must be taken interpreting the Burgers vector type and character of each zig or zag.

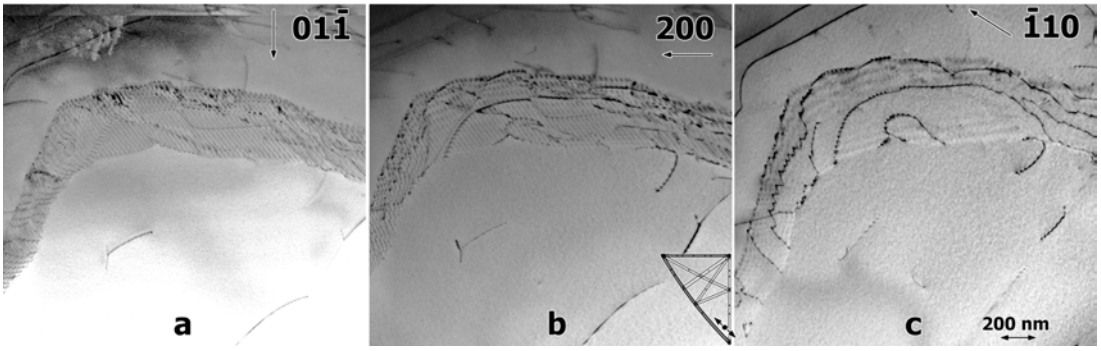

Figure 7. An adjacent sub-grain boundary in condition AR-16 at 800ºC and 77 MPa.

Discussion

The results of microstructural examinations of these V-4Cr-4Ti pressurized thermal creep tubes provide insight into the deformation mechanisms controlling creep behavior at high temperatures. Although higher stress samples showed that the motion of individual dislocations caused the deformation, at lower stresses, deformation arises from flow within grains that is largely restricted to sub-grain boundaries.

The stress dependence of the sub-grain size is often found to vary according to the relation

$$\frac{d_s}{b} = K\left(\frac{G}{\sigma}\right)^m$$

where d_s is the subgrain diameter, b is the Burgers vector, in this case $\frac{a}{2}$<111>, σ is the applied stress, G is the shear modulus and K and m are constants. For pure vanadium, m was estimated at 0.26 and K at 705 for d_s/b in the range 8.4 x 10^3 to 3.0 x 10^3,[4,5] whereas K is very often assumed to be a universal constant of the order of 20 and m approximately 1.[6]

An estimate for K for V-4Cr-4Ti can be made based on the present work. For AR-16 at 800ºC and 70.6 MPa, based on Figure 3, d_s is estimated at 1000nm. Then G can be estimated at 39.4 GPa based on [7], and b at 0.262 nm based on pure vanadium, allowing estimate of K at 6.8 if m = 1, or 735 if m = 0.26. The latter agreement with values for pure vanadium is perhaps remarkable.

Conclusions

Thermal creep at 700 and 800ºC is controlled by dislocation climb. At higher stresses, dislocations move individually and motion may be affected by precipitation. At lower stress, dislocations form sub-grain boundary arrays with mis-orientation developed across the boundary. Therefore, the deformation at lower stresses is expected to be controlled by climb of dislocations into and within the sub-grain boundaries. The present results are shown to agree well with those for pure vanadium regarding the expected stress dependence of the sub-grain size.

FUTURE WORK

This work will be continued when more specimens are available for testing. Specimens irradiated in HFIR at 500°C would be appropriate.

REFERENCES

[1] D. S. Gelles, M. L. Hamilton and R. J. Kurtz, DOE/ER-0313/26 (1999) 11.

[2] R. J. Kurtz and M. L. Hamilton, DOE/ER-0313/26 (1999) 11.

[3] D. S. Gelles, A. Kimura and R. J. Puigh, DOE/ER-0313/25 (1999) 7.

[4] V. V. Levitin, Phys. Stat. Sol., (a) 62 (1980) 557.

[5] S. V. Raj and G. M. Pharr, Mater. Sci. Eng., 81 (1986) 217.

[6] L.P. Kubin, *Dislocation patterning.* Mater. Sci. Technol., 6 **(**1993) 137.

[7] W. E. Porter, R. B. Dinwiddie, W. A. Simpson and M. L. Grossbeck, ANL/FPP/TM-287 (1994) 41.